JOURNAL OF GUIDANCE, CONTROL, AND DYNAMICS
Vol. 36, No. 3, May–June 2013

Waypoint-Optimized Zero-Effort-Miss/Zero-Effort-Velocity Feedback Guidance for Mars Landing

Yanning Guo,* Matt Hawkins,† and Bong Wie‡
Iowa State University, Ames, Iowa 50010-2271

DOI: 10.2514/1.58098

This paper investigates the optimization approach to generate waypoints for the Mars landing problem in the context of employing the zero-effort-miss/zero-effort-velocity feedback guidance algorithm. For a power-limited engine, the waypoint optimization problem in the presence of state constraints is converted to an equivalent standard quadratic programming problem, which can be solved efficiently. In the case with a thrust-limited engine, by introducing a continuously differentiable function to approximate the standard saturation function, the optimal waypoint can be determined using open-source optimization software. This novel idea exploits parameter optimization techniques for feedback control implementation, thus, it can combine the advantages of open-loop and closed-loop methods to achieve near-optimal performance with acceptable robustness, while meeting various practical constraints and requirements.

I. Introduction

THE Mars pinpoint landing problem continues to be an active area of research. A considerable amount of effort has been devoted to it, with many new issues being investigated. The general Mars entry, descent, and landing (EDL) mission is divided into four phases: the hypersonic entry phase, the subsonic parachute entry phase, the propulsive terminal descent (or powered descent) phase, and the touchdown phase [1,2]. Due to the difficulty of accounting for accumulated uncertainties from the first two phases, past landing missions, including the Viking series (launched in 1975), Mars Pathfinder (1996), and Mars Exploration Rover (2003), focused only on a safe landing. Landing accuracies larger than 10 km were acceptable for these missions. Even the recent Phoenix lander (2007) used a gravity turn descent, because precision landing is not required [3]. The Mars Science Laboratory (launched on 26 November 2011) is expected to use a precision EDL system to reach a more scientifically interesting area with hazardous terrain nearby and to demonstrate advanced landing capabilities.

Açikmeşe and Ploen presented an offline convex optimization approach for fuel-optimal Mars pinpoint landing [4]. This approach takes many complex constraints into account, especially the nonconvex lower bound on thruster levels. The approach was extended to a minimum landing error problem for the case where no feasible pinpoint landing trajectories exist [5]. These approaches, however, are not robust against disturbances, and require precise mathematical modeling. Their open-loop natures make them inapplicable for autonomous onboard implementation, given the wide range of potential initial conditions and the short propulsive terminal descent phase.

Ebrahimi et al. proposed a robust optimal sliding mode guidance law for an exoatmospheric interceptor, using fixed-interval propulsive maneuvers [6]. In this paper, gravity was considered to be a pure function of time. One major contribution of Ebrahimi et al. was the new concept of the zero-effort-velocity (ZEV) error, analogous to the well-known zero-effort-miss (ZEM) distance. The ZEV is the velocity error at the end of the mission if no further control accelerations are imparted. Furfaro et al. later employed the ZEM/ZEV concept to construct two classes of nonlinear guidance algorithms for a lunar precision landing mission [7]. The performance of the ZEM/ZEV algorithm for an asteroid intercept mission with precision targeting requirements was evaluated by Hawkins et al. [8], and compared with the performances of classical missile guidance methods like proportional navigation guidance (PNG) and augmented PNG. Reference [9] showed that in a uniform gravitational field, the ZEM/ZEV algorithm is equivalent to well-known classical optimal feedback controllers for problems such as intercept or rendezvous [10], terminal guidance [11], and planetary landing [12,13].

All of the optimal feedback guidance algorithms just discussed are concerned only with the specified boundary conditions. For the Mars landing problem, this is not sufficient. For example, the basic ZEM/ZEV algorithm does not ensure that a lander will stay above the surface of Mars for the duration of the mission. The ZEM/ZEV algorithm, then, must be adapted to avoid collision with the surface of Mars, or other constraints.

Steinfeldt et al. describe a method of adjusting the flight time to meet constraints on control magnitude and altitude [13]. Changing only the flight time, however, is of limited utility when dealing with landing mission constraints. Control saturation limits can be alleviated by increasing the mission time, so that the same total amount of control effort can be distributed over a longer period. Collision avoidance, especially avoiding collision with the surface, can usually be achieved by reducing the mission time, driving the lander closer to a "straight shot" trajectory. These contradictory demands cannot both be satisfied by changing the mission flight time.

In general, a Mars lander should be able to predict its trajectory and evaluate the possibility of impact during the flight. If a hazard is detected, effective measures can be taken. Guo et al. [9] include an exploratory study of waypoint guidance, choosing a waypoint as an intermediate target to meet mission constraints. Near-optimal performance can be achieved with only one waypoint. In this study, however, the waypoint was chosen by trial and error, and a more rigorous, autonomous method is needed. The waypoint method is also studied by Sharma et al. [14] as a means to solve nonlinear optimal control problems with terminal constraints.

In the last decade pseudospectral optimization methods have been used for a variety of optimal control applications [15–17]. NASA's Transition Region and Corona Explorer spacecraft successfully flight-tested time-optimal slews in the presence of various constraints, ushering in a new era of employing optimization techniques

Received 28 February 2012; revision received 8 August 2012; accepted for publication 16 August 2012; published online 21 February 2013.

*Visiting Student, Department of Aerospace Engineering; currently Ph.D. Candidate, Department of Control Science and Engineering, Harbin Institute of Technology, 150001 Harbin, People's Republic of China.

†Ph.D. Candidate, Department of Aerospace Engineering, 2271 Howe Hall, Room 2348.

‡Vance Coffman Endowed Chair Professor, Asteroid Deflection Research Center, Department of Aerospace Engineering, 2271 Howe Hall, Room 2355.

for advanced space missions [18]. A number of optimization software packages are now on the market, including SNOPT, DIDO, TOMLAB [19], and others. General Pseudospectral Optimal Control Software (GPOPS) is one of the most versatile open-source multiphase optimizers using pseudospectral methods and is used in this paper. Its latest version offers a mesh refinement algorithm to accurately distribute collocation points [20]. This paper begins with a brief summary of optimal ZEM/ZEV algorithms. Key results are given, including a method for determining time-to-go. Two types of spacecraft engine are considered. First is a power-limited engine. The total flight time is divided into two parts, with the acceleration assumed to be a linear function of time in each segment. The state constraint is considered as an inequality constraint, and the waypoint optimization problem becomes a standard quadratic programming problem. Although the power-limited engine may be impractical to be employed for Mars landing, it is used here to illustrate the applicability of the ZEM/ZEV method for different thruster systems, but not necessarily as a practical mission example. For the thrust-limited engine, GPOPS is used to determine optimal waypoints. GPOPS is suitable for constraining the control commands to be a function the current and terminal states. To improve the efficiency and accuracy of the optimization, a continuously differentiable function is developed that approaches the classical saturation function, so that analytical derivatives can be passed to GPOPS. The novelty of this waypoint research lies in the combination of the optimal properties of the optimization approach and the robustness of ZEM/ZEV feedback control. Numerical simulations confirm the effectiveness of this approach.

II. Equations of Motion

Neglecting aerodynamic drag, the trajectory equations of motion during the powered descent phase for a Mars lander are described by

$$\dot{\mathbf{r}} = \mathbf{v} \tag{1}$$

$$\dot{\mathbf{v}} = \mathbf{g} + \mathbf{a} \tag{2}$$

$$\mathbf{a} = \frac{\mathbf{T}}{m} \tag{3}$$

where $\mathbf{r}$ and $\mathbf{v}$ are the position and velocity vectors, $\mathbf{a}$ is the control acceleration provided by the thrusters, $\mathbf{T}$ is the thrusting force vector, m is the spacecraft mass, and $\mathbf{g}$ is the gravitational acceleration vector acting on the vehicle. During the powered descent phase, $\mathbf{g}$ is considered to be constant. These vectors are 3×1 column vectors expressed in a nonrotating inertial reference frame with its origin at the landing site of Mars.

The magnitude of the thrusting force T is modeled as the two-norm of a vector $\mathbf{T}$ as

$$T = |\mathbf{T}| = -\dot{m}c \tag{4}$$

where $\dot{m}$ is the negative mass flow rate, and $c = I_{\text{sp}} g_0$ is the engine exhaust velocity.

A. Optimal Feedback Guidance Algorithms

Consider a classical optimization problem with the following performance index:

$$J = \frac{1}{2}\int_{t_0}^{t_f} \mathbf{a}^T \mathbf{a}\, \mathrm{d}t \tag{5}$$

subject to Eqs. (1) through (4) and the following boundary conditions:

$$\begin{aligned} \mathbf{r}(t_0) &= \mathbf{r}_0 = [x_0 \quad y_0 \quad z_0]^T, & \mathbf{r}(t_f) &= \mathbf{r}_f = [x_f \quad y_f \quad z_f]^T \\ \mathbf{v}(t_0) &= \mathbf{v}_0 = [\dot{x}_0 \quad \dot{y}_0 \quad \dot{z}_0]^T, & \mathbf{v}(t_f) &= \mathbf{v}_f = [\dot{x}_f \quad \dot{y}_f \quad \dot{z}_f]^T \end{aligned} \tag{6}$$

The Hamiltonian function is defined as

$$H = \frac{1}{2}\mathbf{a}^T\mathbf{a} + \mathbf{p}_r^T\mathbf{v} + \mathbf{p}_v^T(\mathbf{g} + \mathbf{a}) \tag{7}$$

where $\mathbf{p}_r$ and $\mathbf{p}_v$ are the costate vectors associated with the position and velocity vectors, respectively.

From the costate equations, the optimal control solution can be expressed as a linear combination of the terminal value of costate vectors as

$$\mathbf{a} = -t_{\text{go}}\mathbf{p}_r(t_f) - \mathbf{p}_v(t_f) \tag{8}$$

where the time-to-go t_{go} is defined as: $t_{\text{go}} = t_f - t$.

By substituting this expression into the dynamic equations and solving for $\mathbf{p}_r(t_f)$ and $\mathbf{p}_v(t_f)$, the optimal control law with the specified $\mathbf{r}_f$, $\mathbf{v}_f$, and t_f is obtained as

$$\mathbf{a} = \frac{6[\mathbf{r}_f - (\mathbf{r} + t_{\text{go}}\mathbf{v})]}{t_{\text{go}}^2} - \frac{2(\mathbf{v}_f - \mathbf{v})}{t_{\text{go}}} - \mathbf{g} \tag{9}$$

The ZEM distance and ZEV error denote the differences between the desired final position and velocity and the projected final position and velocity if no additional control is commanded after the current time. For the assumed constant gravitational acceleration, the ZEM and ZEV have the following expressions [6–9]:

$$\mathbf{ZEM} = \mathbf{r}_f - \left(\mathbf{r} + t_{\text{go}}\mathbf{v} + \frac{1}{2}t_{\text{go}}^2\mathbf{g}\right) \tag{10}$$

$$\mathbf{ZEV} = \mathbf{v}_f - (\mathbf{v} + t_{\text{go}}\mathbf{g}) \tag{11}$$

Using these expressions, Eq. (9) can be rewritten as

$$\mathbf{a} = \frac{6}{t_{\text{go}}^2}\mathbf{ZEM} - \frac{2}{t_{\text{go}}}\mathbf{ZEV} \tag{12}$$

For the Mars soft landing problem, the landing site is typically chosen as the origin of the reference frame, and therefore $\mathbf{r}_f = 0$, $\mathbf{v}_f = 0$, the optimal guidance law has the well-known simple form [1,12]:

$$\mathbf{a} = -\frac{6\mathbf{r}}{t_{\text{go}}^2} - \frac{4\mathbf{v}}{t_{\text{go}}} - \mathbf{g} \tag{13}$$

B. Determination of Time-to-Go

The optimal mission time-to-go can be determined as the minimum real positive solution of the following equation [9]:

$$\begin{aligned} &\mathbf{g}^T\mathbf{g}t_{\text{go}}^4 - 4(\mathbf{v}^T\mathbf{v} + \mathbf{v}_f^T\mathbf{v} + \mathbf{v}_f^T\mathbf{v}_f)t_{\text{go}}^2 \\ &\quad + 24(\mathbf{r}_f - \mathbf{r})^T(\mathbf{v} + \mathbf{v}_f)t_{\text{go}} - 36(\mathbf{r}_f - \mathbf{r})^T(\mathbf{r}_f - \mathbf{r}) = 0 \end{aligned} \tag{14}$$

Equation (14) can be simplified for the Mars soft landing problem due to the simple terminal state requirements, as follows:

$$\mathbf{g}^T\mathbf{g}t_{\text{go}}^4 - 4\mathbf{v}^T\mathbf{v}t_{\text{go}}^2 - 24\mathbf{r}^T\mathbf{v}t_{\text{go}} - 36\mathbf{r}^T\mathbf{r} = 0 \tag{15}$$

The altitude component of the vehicle's position can thus be expressed as

$$y(t) = -\frac{(t_f - t)^3}{6} p_{ry} + \frac{(t_f - t)^2}{2}(g - p_{vy}) \tag{16}$$

where y is the altitude of the vehicle, g is the gravitational acceleration, and p_{ry} and p_{vy} are the components of the costate vectors along the altitude direction, given by

$$p_{ry} = \frac{6\dot{y}_0}{t_f^2} + \frac{12 y_0}{t_f^3} \tag{17}$$

$$p_{vy} = -\frac{2\dot{y}_0}{t_f} - \frac{6 y_0}{t_f^2} + g \tag{18}$$

The upper limit on flight time, which ensures a positive altitude in the time period $(0, t_f)$, can be found by analyzing the distribution of the roots of Eq. (16), which gives

$$t_{\max} = -\frac{3 y_0}{\dot{y}_0} \tag{19}$$

If the optimal t_f obtained from Eq. (15) exceeds the upper limit $t_{\max}$ from Eq. (19), the lander will collide with Mars's surface before the scheduled landing at t_f. When a collision is predicted, the final time can be adjusted to $t_{\max}$ to complete the landing mission without collision, at the expense of a higher performance index value.

When there is a constraint on either the control force or the control acceleration, adjusting the flight time is usually not sufficient. To overcome this defect, the waypoint-optimized ZEM/ZEV feedback scheme is proposed in the next section.

III. Waypoint Optimization for Power-Limited Engine

For a power-limited (or variable specific impulse) engine, the power for a given thrust T is expressed as [21–23]

$$P = -\frac{1}{2}\dot{m}c^2 = \frac{1}{2}cT = -\frac{1}{2}\frac{m^2}{\dot{m}}|\mathbf{a}|^2 \le P_{\max} \tag{20}$$

where $P_{\max}$ is the maximum power available from the engine.

The performance index can be expressed in terms of the final mass of the spacecraft by integrating Eq. (20) as follows:

$$J = \frac{1}{2}\int_{t_0}^{t_f} |\mathbf{a}|^2 \,\mathrm{d}t \le -P_{\max}\int_{t_0}^{t_f} \frac{\dot{m}}{m^2}\,\mathrm{d}t = \frac{P_{\max}}{m_f} - \frac{P_{\max}}{m_0} \tag{21}$$

Equation (20) shows that, for a given acceleration command $\mathbf{a}$ and current mass m, a larger power P results in a smaller mass consumption rate $|\dot{m}|$. If the thruster always operates at $P_{\max}$, all of the terms in Eq. (21) are equal, and minimizing J is equivalent to maximizing the final mass of the spacecraft m_f. The ZEM/ZEV algorithm discussed in this paper is thus optimal in terms of mass consumption.

The ZEM/ZEV feedback guidance command for constant gravitational acceleration is a linear function of time. By dividing the mission time into two parts, from the beginning to the waypoint time t_m, and from the waypoint time to the end, the optimal accelerations can be expressed as

$$\mathbf{a} = \begin{cases} (t - t_0)\boldsymbol{\alpha}_1 + \boldsymbol{\beta}_1 - \mathbf{g} & t \in (t_0, t_m) \\ (t_f - t)\boldsymbol{\alpha}_2 + \boldsymbol{\beta}_2 - \mathbf{g} & t \in (t_m, t_f) \end{cases} \tag{22}$$

where $\boldsymbol{\alpha}_1, \boldsymbol{\alpha}_2, \boldsymbol{\beta}_1$, and $\boldsymbol{\beta}_2$ are constant vectors to be found.

Substituting Eq. (22) into the equations of motion, the waypoint velocity and position can be found from successive integrations from t_0 to t_m as

$$\mathbf{v}_m = \frac{1}{2}t_1^2\alpha_1 + t_1\boldsymbol{\beta}_1 + \mathbf{v}_0 \tag{23}$$

$$\mathbf{r}_m = \frac{1}{6}t_1^3\alpha_1 + \frac{1}{2}t_1^2\boldsymbol{\beta}_1 + \mathbf{v}_0 t_1 + \mathbf{r}_0 \tag{24}$$

where time duration of the segment is defined as $t_1 = t_m - t_0$.

The waypoint velocity and position can be found similarly for the second segment as

$$\mathbf{v}_m = -\frac{1}{2}t_2^2\alpha_2 - t_2\boldsymbol{\beta}_2 + \mathbf{v}_f \tag{25}$$

$$\mathbf{r}_m = \frac{1}{6}t_2^3\alpha_2 + \frac{1}{2}t_2^2\boldsymbol{\beta}_2 - \mathbf{v}_f t_2 + \mathbf{r}_f \tag{26}$$

where $t_2 = t_f - t_m$.

Combining Eqs. (23–26) leads to the following boundary conditions:

$$\mathbf{v}_f - \mathbf{v}_0 = \frac{1}{2}t_1^2\alpha_1 + \frac{1}{2}t_2^2\alpha_2 + t_1\boldsymbol{\beta}_1 + t_2\boldsymbol{\beta}_2 \tag{27}$$

$$\mathbf{v}_0 t_1 + \mathbf{v}_f t_2 - \mathbf{r}_f + \mathbf{r}_0 = -\frac{1}{6}t_1^3\alpha_1 + \frac{1}{6}t_2^3\alpha_2 - \frac{1}{2}t_1^2\boldsymbol{\beta}_1 + \frac{1}{2}t_2^2\boldsymbol{\beta}_2 \tag{28}$$

The performance index, defined as Eq. (5), can now be expressed in terms of the unknown parameters $\alpha_1, \alpha_2, \boldsymbol{\beta}_1$, and $\boldsymbol{\beta}_2$ as

$$\begin{aligned} J &= \frac{1}{2}\int_{t_0}^{t_f} \mathbf{a}^T\mathbf{a}\,\mathrm{d}t = \frac{1}{2}\int_{t_0}^{t_m} \mathbf{a}^T\mathbf{a}\,\mathrm{d}t + \frac{1}{2}\int_{t_m}^{t_f} \mathbf{a}^T\mathbf{a}\,\mathrm{d}t \\ &= \frac{1}{2}\left\{\begin{array}{l} \frac{1}{3}\boldsymbol{\alpha}_1^T\alpha_1 t_1^3 + \boldsymbol{\alpha}_1^T(\boldsymbol{\beta}_1 - \mathbf{g})t_1^2 + \frac{1}{3}\boldsymbol{\alpha}_2^T\alpha_2 t_2^3 + \boldsymbol{\alpha}_2^T(\boldsymbol{\beta}_2 - \mathbf{g})t_2^2 \\ +(\boldsymbol{\beta}_1 - \mathbf{g})^T(\boldsymbol{\beta}_1 - \mathbf{g})t_1 + (\boldsymbol{\beta}_2 - \mathbf{g})^T(\boldsymbol{\beta}_2 - \mathbf{g})t_2 \end{array}\right\} \end{aligned} \tag{29}$$

Define $\mathbf{x} = [\boldsymbol{\alpha}_1^T \quad \alpha_2^T \quad \boldsymbol{\beta}_1^T \quad \boldsymbol{\beta}_2^T]^T$ as the vector of to-be-determined constants. The waypoint optimization problem can now be described as a standard quadratic programming problem, where the goal is to determine a vector $\mathbf{x}$, which minimizes the following function:

$$J = \frac{1}{2}\mathbf{x}^T\mathbf{H}\mathbf{x} + \mathbf{c}^T\mathbf{x} \tag{30}$$

where

$$\mathbf{H} = \begin{bmatrix} \frac{1}{3}t_1^3\mathbf{I}_3 & 0_3 & \frac{1}{2}t_1^2\mathbf{I}_3 & 0_3 \\ 0_3 & \frac{1}{3}t_2^3\mathbf{I}_3 & 0_3 & \frac{1}{2}t_2^2\mathbf{I}_3 \\ \frac{1}{2}t_1^2\mathbf{I}_3 & 0_3 & \frac{1}{2}t_1^2\mathbf{I}_3 & 0_3 \\ 0_3 & \frac{1}{2}t_2^2\mathbf{I}_3 & 0_3 & t_2\mathbf{I}_3 \end{bmatrix}, \qquad \mathbf{c} = -\begin{bmatrix} \frac{1}{2}t_1^2\mathbf{g} \\ \frac{1}{2}t_2^2\mathbf{g} \\ t_1\mathbf{g} \\ t_2\mathbf{g} \end{bmatrix}$$

subject to one or more constraints of the form

$$\mathbf{A}_{\mathrm{eq}}\mathbf{x} = \mathbf{b}_{\mathrm{eq}} \tag{31}$$

$$\mathbf{A}_{\mathrm{ineq}}\mathbf{x} \le \mathbf{b}_{\mathrm{ineq}} \tag{32}$$

where $\mathbf{I}_3$ is the 3×3 identity matrix, and 0_3 is the 3×3 zero matrix.

The boundary condition given by Eqs. (27) and (28) is an equality constraint, which can be cast in the standard form of Eq. (31) as

$$\mathbf{A}_{\mathrm{eq}} = \begin{bmatrix} \frac{1}{2}t_1^2\mathbf{I}_3 & \frac{1}{2}t_2^2\mathbf{I}_3 & t_1\mathbf{I}_3 & t_2\mathbf{I}_3 \\ -\frac{1}{6}t_1^3\mathbf{I}_3 & \frac{1}{6}t_2^3\mathbf{I}_3 & -\frac{1}{2}t_1^2\mathbf{I}_3 & \frac{1}{2}t_2^2\mathbf{I}_3 \end{bmatrix},$$

$$\mathbf{b}_{\mathrm{eq}} = \begin{bmatrix} \mathbf{v}_f - \mathbf{v}_0 \\ \mathbf{v}_0 t_1 + \mathbf{v}_f t_2 - \mathbf{r}_f + \mathbf{r}_0 \end{bmatrix}$$

Altitude constraints, such as the no-subsurface flight constraint, or a glide-slope constraint, are inequality constraints. For brevity, in this example we look in detail at only the no-subsurface flight constraint. Other inequality constraints can be handled similarly.

Let us divide the two mission segments into N_1 and N_2 equal intervals, respectively. Let $a_i = (i \cdot t_1)/N_1,\ (i = 1, 2, \ldots, N_1)$ denote the duration of each interval in the first mission segment, and $(b_i = (t_f - j \cdot t_2)/N_2,\ (j = 1, 2, \ldots, N_2 - 1)$ denote the duration of each interval in the second mission segment. The no-subsurface flight constraint is thus described by:

$$\begin{bmatrix} 0 \\ 1 \\ 0 \end{bmatrix}^T \left(\frac{1}{6} a_i^3 \alpha_1 + \frac{1}{2} a_i^2 \boldsymbol{\beta}_1 + a_i \mathbf{v}_0 + \mathbf{r}_0 \right) \geq 0 \qquad i = 1, 2, \ldots, N_1 \tag{33}$$

$$\begin{bmatrix} 0 \\ 1 \\ 0 \end{bmatrix}^T \left(\frac{1}{6} b_j^3 \alpha_2 + \frac{1}{2} b_j^2 \boldsymbol{\beta}_2 - b_j \mathbf{v}_f + \mathbf{r}_f \right) \geq 0$$
$$j = 1, 2, \ldots, N_2 - 1 \tag{34}$$

Equations (33) and (34) describe a total of $N_1 + N_2 - 1$ inequality constraints. These constraints can be cast in the standard form of Eq. (32) as

$$\mathbf{A}_{\text{ineq}} = -\begin{bmatrix} 0 & \frac{1}{6}a_1^3 & 0 & 0 & 0 & 0 & 0 & \frac{1}{2}a_1^2 & 0 & 0 & 0 & 0 \\ \vdots & \vdots & \vdots & \vdots & \vdots & \vdots & \vdots & \vdots & \vdots & \vdots & \vdots & \vdots \\ 0 & \frac{1}{6}a_{N_1}^3 & 0 & 0 & 0 & 0 & 0 & \frac{1}{2}a_{N_1}^2 & 0 & 0 & 0 & 0 \\ 0 & 0 & 0 & 0 & \frac{1}{6}b_1^3 & 0 & 0 & 0 & 0 & 0 & \frac{1}{2}b_1^2 & 0 \\ \vdots & \vdots & \vdots & \vdots & \vdots & \vdots & \vdots & \vdots & \vdots & \vdots & \vdots & \vdots \\ 0 & 0 & 0 & 0 & \frac{1}{6}b_{N_2-1}^3 & 0 & 0 & 0 & 0 & 0 & \frac{1}{2}b_{N_2-1}^2 & 0 \end{bmatrix}_{(N_1+N_2-1)\times 12}$$

$$\mathbf{b}_{\text{ineq}} = [\, y_0 + a_1\dot{y}_0 \quad \cdots \quad y_0 + a_{N1}\dot{y}_0 \quad y_f - \dot{y}_f b_1 \quad \ldots \quad y_f - \dot{y}_f b_{N_2-1} \,]^T_{(N_1+N_2-1)\times 1}$$

The minimum altitude constraints, as well as glide slope constraint, etc., can similarly be expressed in the form of Eq. (32). Details are omitted here.

A number of commercially available programs can solve this quadratic programming problem. Once the minimizing vector $\mathbf{x}$ is found, the waypoint velocity and position can be found from either Eqs. (23) and (24), or Eqs. (25) and (26). This approach can be extended to include multiple waypoints, with each additional waypoint increasing the size of the unknown vector.

IV. Waypoint Optimization for Thrust-Limited Engine

For a spacecraft equipped with a thrust-limited engine, the engine exhaust velocity is fixed at a constant value. The thrust magnitude is constrained as

$$0 \leq T \leq T_{\max} \tag{35}$$

where $T_{\max}$ is the maximum available thrust.

Considering control saturation, the ZEM/ZEV algorithm given by Eq. (12) becomes

$$\mathbf{a} = \underset{T_{\max}/m}{\text{sat}} \left(\frac{6}{t_{\text{go}}^2} \mathbf{ZEM} - \frac{2}{t_{\text{go}}} \mathbf{ZEV} \right) \tag{36}$$

where the normalized saturation function of a vector $\mathbf{q}$ is defined as

$$\underset{U}{\text{sat}}(\mathbf{q}) = \begin{cases} \mathbf{q} & \text{if } |\mathbf{q}| \leq U \\ \mathbf{q}\frac{U}{|\mathbf{q}|} & \text{if } |\mathbf{q}| U \end{cases} \tag{37}$$

The normalized saturation function, given by Eq. (37), is non-differentiable at the critical saturation points. Typical optimization packages, such as GPOPS, can make use of analytical partial derivatives of the constraints with respect to the states and controls. Supplying these derivatives can greatly improve the computational efficiency and accuracy of the optimization problem. The following continuously differentiable function approximates the saturation function:

$$\underset{U}{\text{sat}}(\mathbf{q}) = \begin{cases} \mathbf{q} & \text{if } \frac{U}{|\mathbf{q}|} > n_U \\ \Phi(\mathbf{q}, U) \cdot \mathbf{q} & \text{if } \frac{U}{|\mathbf{q}|} \in [n_L, n_U] \\ \frac{U}{|\mathbf{q}|} \cdot \mathbf{q} & \text{if } \frac{U}{|\mathbf{q}|} < n_L \end{cases} \tag{38}$$

where the function Φ is a second-order spline function whose coefficients depend on the endpoints of the interval. The modified saturation function becomes the normalized saturation function when the interval (n_L, n_U) shrinks to zero. For this study, the interval is chosen as (0.9, 1.1). Then we have

$$\Phi(\mathbf{q}, U) = -2.5\left(\frac{U}{|\mathbf{q}|}\right)^2 + 5.5\frac{U}{|\mathbf{q}|} - 2.025 \tag{39}$$

$$\frac{\partial \underset{U}{\text{sat}}(\mathbf{q})}{\partial \mathbf{q}} = \begin{cases} \mathbf{I}_3 & \text{if } \frac{U}{|\mathbf{q}|} > 1.1 \\ \Phi(\mathbf{q}, U) \cdot \mathbf{I}_3 + \frac{U}{|\mathbf{q}|}\left(5\frac{U}{|\mathbf{q}|} - 5.5\right) \cdot \frac{\mathbf{q}\mathbf{q}^T}{|\mathbf{q}|^2} & \text{if } \frac{U}{|\mathbf{q}|} \in [0.9, 1.1] \\ \frac{U}{|\mathbf{q}|}\left(\mathbf{I}_3 - \frac{\mathbf{q}\mathbf{q}^T}{|\mathbf{q}|^2}\right) & \text{if } \frac{U}{|\mathbf{q}|} < 0.9 \end{cases} \tag{40}$$

where the continuity of Eq. (40) can be easily verified.

The waypoint optimization problem for a thrust-limited engine becomes:

Determine the optimal waypoint ($\mathbf{r}_m$ and $\mathbf{v}_m$) to connect the following two phases:

$$\begin{aligned} &\text{Phase 1}(t_0 \leq t \leq t_m) \begin{cases} \mathbf{r}(t_0) = \mathbf{r}_0, \quad \mathbf{r}(t_m) = \mathbf{r}_m = \text{free} \\ \mathbf{v}(t_0) = \mathbf{v}_0, \quad \mathbf{v}(t_m) = \mathbf{v}_m = \text{free} \end{cases} \\ &\text{Phase 2}(t_m \leq t \leq t_f) \begin{cases} \mathbf{r}(t_m) = \mathbf{r}_m = \text{free}, \quad \mathbf{r}(t_f) = \mathbf{r}_f \\ \mathbf{v}(t_m) = \mathbf{v}_m = \text{free}, \quad \mathbf{v}(t_f) = \mathbf{v}_f \end{cases} \end{aligned} \tag{41}$$

where each phase is governed by Eqs. (1–4), and the acceleration command is assumed to have the following form:

$$\begin{aligned} &\text{Phase 1}(t_0 \leq t \leq t_m) \qquad \mathbf{a} = \underset{T_{\max}/m}{\text{sat}}(\mathbf{a}_{c1}) \\ &\text{Phase 2}(t_m \leq t \leq t_f) \qquad \mathbf{a} = \underset{T_{\max}/m}{\text{sat}}(\mathbf{a}_{c2}) \end{aligned} \tag{42}$$

where

$$\mathbf{a}_{c1} = \frac{6(\mathbf{r}_m - \mathbf{r})}{(t_m - t)^2} - \frac{2\mathbf{v}_m + 4\mathbf{v}}{t_m - t} - \mathbf{g} \quad \mathbf{a}_{c2} = -\frac{6\mathbf{r}}{(t_f - t)^2} - \frac{4\mathbf{v}}{t_f - t} - \mathbf{g}$$

and the following path constraints are satisfied during the two phases

$$\begin{aligned} &\text{Phase 1}(t_0 \le t \le t_m) \qquad \boldsymbol{\sigma}_{c1} \equiv \mathbf{a} - \underset{T_{\max}/m}{\text{sat}}(\mathbf{a}_{c1}) \\ &\text{Phase 2}(t_m \le t \le t_f) \qquad \boldsymbol{\sigma}_{c2} \equiv \mathbf{a} - \underset{T_{\max}/m}{\text{sat}}(\mathbf{a}_{c2}) \end{aligned} \tag{43}$$

where the path constraints, $\boldsymbol{\sigma}_{c1}$ and $\boldsymbol{\sigma}_{c2}$, must be zero during the entire phase.

The derivatives of the dynamic equations and the cost function are straightforward to find. Note that the path constraints in the two phases are the same. The partial derivatives of the path constraints will be given for phase 1. The partial derivatives for phase 2 proceed similarly.

$$\frac{\partial \boldsymbol{\sigma}_{c1}}{\partial \mathbf{a}} = \mathbf{I}_3 \tag{44}$$

$$\frac{\partial \boldsymbol{\sigma}_{c1}}{\partial \mathbf{r}} = -\frac{\partial \underset{T_{\max}/m}{\text{sat}}(\mathbf{a}_1)}{\partial \mathbf{a}_1} \cdot \frac{\partial \mathbf{a}_1}{\partial \mathbf{r}} = \frac{\partial \underset{T_{\max}/m}{\text{sat}}(\mathbf{a}_1)}{\partial \mathbf{a}_1} \cdot \frac{6}{(t_m - t)^2} \mathbf{I}_3 \tag{45}$$

$$\frac{\partial \boldsymbol{\sigma}_{c1}}{\partial \mathbf{r}_m} = -\frac{\partial \underset{T_{\max}/m}{\text{sat}}(\mathbf{a}_1)}{\partial \mathbf{a}_1} \cdot \frac{\partial \mathbf{a}_1}{\partial \mathbf{r}_m} = \frac{\partial \underset{T_{\max}/m}{\text{sat}}(\mathbf{a}_1)}{\partial \mathbf{a}_1} \cdot \frac{-6}{(t_m - t)^2} \mathbf{I}_3 \tag{46}$$

$$\frac{\partial \boldsymbol{\sigma}_{c1}}{\partial \mathbf{v}} = -\frac{\partial \underset{T_{\max}/m}{\text{sat}}(\mathbf{a}_1)}{\partial \mathbf{a}_1} \cdot \frac{\partial \mathbf{a}_1}{\partial \mathbf{v}} = \frac{\partial \underset{T_{\max}/m}{\text{sat}}(\mathbf{a}_1)}{\partial \mathbf{a}_1} \cdot \frac{4}{t_m - t} \mathbf{I}_3 \tag{47}$$

$$\frac{\partial \boldsymbol{\sigma}_{c1}}{\partial \mathbf{v}_m} = -\frac{\partial \underset{T_{\max}/m}{\text{sat}}(\mathbf{a}_1)}{\partial \mathbf{a}_1} \cdot \frac{\partial \mathbf{a}_1}{\partial \mathbf{v}_m} = \frac{\partial \underset{T_{\max}/m}{\text{sat}}(\mathbf{a}_1)}{\partial \mathbf{a}_1} \cdot \frac{2}{t_m - t} \mathbf{I}_3 \tag{48}$$

$$\begin{aligned} \frac{\partial \boldsymbol{\sigma}_{c1}}{\partial t} &= -\frac{\partial \underset{T_{\max}/m}{\text{sat}}(\mathbf{a}_1)}{\partial \mathbf{a}_1} \cdot \frac{\partial \mathbf{a}_1}{\partial t} \\ &= -\frac{\partial \underset{T_{\max}/m}{\text{sat}}(\mathbf{a}_1)}{\partial \mathbf{a}_1} \cdot \left(\frac{12(\mathbf{r}_m - \mathbf{r})}{(t_m - t)^3} - \frac{2\mathbf{v}_m + 4\mathbf{v}}{(t_m - t)^2} \right) \end{aligned} \tag{49}$$

$$\begin{aligned} \frac{\partial \boldsymbol{\sigma}_{c1}}{\partial t_m} &= -\frac{\partial \underset{T_{\max}/m}{\text{sat}}(\mathbf{a}_1)}{\partial \mathbf{a}_1} \cdot \frac{\partial \mathbf{a}_1}{\partial t_m} \\ &= -\frac{\partial \underset{T_{\max}/m}{\text{sat}}(\mathbf{a}_1)}{\partial \mathbf{a}_1} \cdot \left(-\frac{12(\mathbf{r}_m - \mathbf{r})}{(t_m - t)^3} + \frac{2\mathbf{v}_m + 4\mathbf{v}}{(t_m - t)^2} \right) \end{aligned} \tag{50}$$

The partial derivative of the path constraint with respect to mass can be obtained by referring to Eq. (40). It is omitted here due to the lengthiness of the expression.

More waypoints can be obtained by considering more phases in GPOPS, and increasing the number of waypoints would improve the optimality and decrease the difference with the open-loop optimal solution, but more processing time would be required.

V. Waypoint-Optimized Zero-Effort-Miss/ Zero-Effort-Velocity Scheme

The complete procedure for conducting a Mars pinpoint landing mission using the waypoint-optimized ZEM/ZEV feedback control scheme is proposed as follows:

1) At the end of the subsonic parachute entry phase, determine a suitable landing site.

2) Using the position and velocity of the lander, solve Eq. (15) to obtain the optimal flight time t_f.

3) For a power-limited engine, t_f is the optimal flight time, which minimizes both J and Δm. Numerically propagate the dynamic system with the ZEM/ZEV algorithm to generate the optimal trajectory.

For a thrust-limited engine, t_f can be considered a reference time. A line search can be implemented to determine the optimal t_f for either J or Δm.

4) If any part of the optimal trajectory violates an altitude constraint, go to step 5. Otherwise, go to step 6.

5) Use the optimization approach discussed in this paper to determine a waypoint to satisfy the altitude constraint. Consider the optimized waypoint as an intermediate target, using the ZEV/ZEM algorithm to reach this waypoint.

6) Finally, use the ZEM/ZEV algorithm to land the vehicle at the designated landing site.

The waypoint optimization step 5 requires a certain amount of computational time if t_m and/or t_f is free. Because this guidance scheme is intended for real-time use, it is not advisable to leave the times as completely free parameters. The process can be made much more efficient if both of them are restricted to narrower ranges. The major challenge in a practical mission is how to quickly find these times for step 5. Based on our experiences with a wide variety of numerical simulations, a reasonable method is to simply use the same t_f found in step 3, and choosing the flight time corresponding to the lowest altitude on the optimal trajectory for t_m.

Even though there is no strict guarantee of optimality, this selection has provided good performance in our simulations, close to the performance with free waypoint and final times. In a practical mission, the spacecraft is descending after the end of the parachute entry phase, so a quick solution is desirable. The waypoint and final times are easily found from previous steps, requiring minimal computation.

Both offline and online waypoint optimization schemes have potential for practical implementation. The conventional offline optimal solution approach stores the entire profile onboard, and loses optimality if the lander deviates from the intended path. The waypoint method only requires a single point to be stored, and due to the feedback nature of the ZEM/ZEV algorithm, it is robust against disturbances. For online autonomous application, the vehicle is controlled by the ZEM/ZEV algorithm with t_f from step 3. If a waypoint is needed, the ZEM/ZEV algorithm switches over to the waypoint-optimized ZEM/ZEV algorithm.

VI. Numerical Simulation Examples

A Mars landing example of [4] was examined for both a power-limited engine and a thrust-limited engine. In addition to the ZEM/ZEV feedback guidance algorithms, open-loop optimal solutions were generated with GPOPS for comparison. A spacecraft similar to the one described in [4] is used with an initial mass of 1905 kg. The initial conditions are given as $\mathbf{r}_0 = (2, \quad 1.5, \quad 0)$ km, $\mathbf{v}_0 = (100, \quad -75, \quad 0)$ m/s. The landing site is at the origin of the reference frame, and for a soft landing the final velocity is zero. The final conditions are thus $\mathbf{r}_f = (0, \quad 0, \quad 0)$ km, $\mathbf{v}_f = (0, \quad 0, \quad 0)$ m/s. The constant gravitational acceleration is assumed as $\mathbf{g} = (0, \quad -3.7114, \quad 0)$ m/s^2. It is assumed that all system states are available without any measurement error.

A. Mars Landing with Power-Limited Engine

The power-limited engine may not be available for an actual Mars landing mission; however, it is considered here for a couple of reasons. First, our main research interest is in planetary landing, so this is a way to look at different engine dynamics within our motivating example. Second, as described previously, fuel usage can be directly minimized, unlike with the thrust-limited engine. This happens when the engine operates at the maximum power level, therefore, for these simulations the engine is assumed to always operate at the maximum power level. The quadratic programming problem for waypoint optimization is solved using the MATLAB

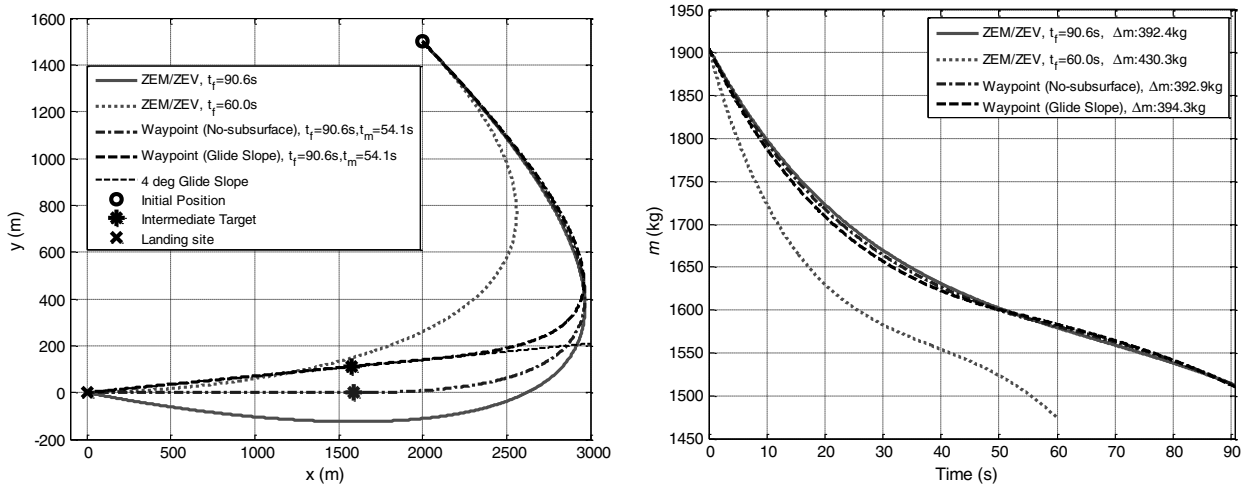

a) Vehicle trajectory **b) Vehicle mass**

Fig. 1 Comparisons of various forms of the ZEM/ZEV algorithm (power-limited engine).

quadprog function with default options. In all test cases the required processing time is less than 0.1 s.

Figure 1 shows the optimal trajectories and corresponding fuel usage histories for the standard ZEM/ZEV algorithm and for the ZEM/ZEV waypoint method with altitude constraints. From step 2 of the landing procedure, the optimal t_f is found to be 90.6 s. Checking Eq. (19) reveals that the upper bound on flight time is 60 s. The solid-line trajectory in Fig. 1 shows that the optimal trajectory for a 90.6 s flight indeed violates the no-subsurface constraint. By adjusting the t_f to 60 s, the ZEM/ZEV algorithm produces the dotted-line trajectory in Fig. 1, which does not violate the constraint. However, the mass usage comparison in Fig. 1 shows that the mission with adjusted flight time uses significantly more fuel.

The waypoint-optimized ZEM/ZEV algorithm can be employed to improve the performance of the mission, while still satisfying the altitude constraints. Following the suggestion for selecting proper waypoint time and final time, the mission time t_f is kept as 90.6 s. From the simulation of the trajectory for the basic ZEM/ZEV algorithm with a 90.6 s mission time, the time corresponding to the minimum altitude is 54.1 s. This is chosen for the waypoint time t_m.

Two types of altitude constraint are considered for the waypoint-optimized ZEM/ZEV method. First is the simple no-subsurface flight constraint, shown as the dash–dot line in Fig. 1. A slightly more sophisticated constraint, keeping the glide slope above 4 deg, is shown by the dashed line. Note that such a constraint automatically satisfies the no-subsurface flight constraint. Figure 1 shows that the fuel usage for both waypoint schemes is nearly identical to the basic optimal ZEM/ZEV algorithm.

Figure 2 shows engine performance histories for the case with one waypoint and a no-subsurface flight constraint, shown as the dash-dot line in Fig. 1. The dotted line in this figure shows the power-limited engine case; the thrust-limited case will be discussed later. The optimal constant power level can be seen, as well as gently changing curves for control magnitude and mass consumption rate. The changing exhaust velocity required for the power-limited engine is also shown.

The waypoint-optimized ZEM/ZEV scheme is intended to be used online, finding the optimal waypoint in real time for a range of possible initial conditions. To demonstrate the applicability of the method for different initial conditions, a range of initial conditions are simulated. The initial velocity and altitude are held constant, while the initial horizontal position ranges from −8 to 3 km. A 50 m minimum altitude is imposed to avoid collision with surface hazards, making the final position $\mathbf{r}_f = (0, \quad 50, \quad 0)$ m. From here the

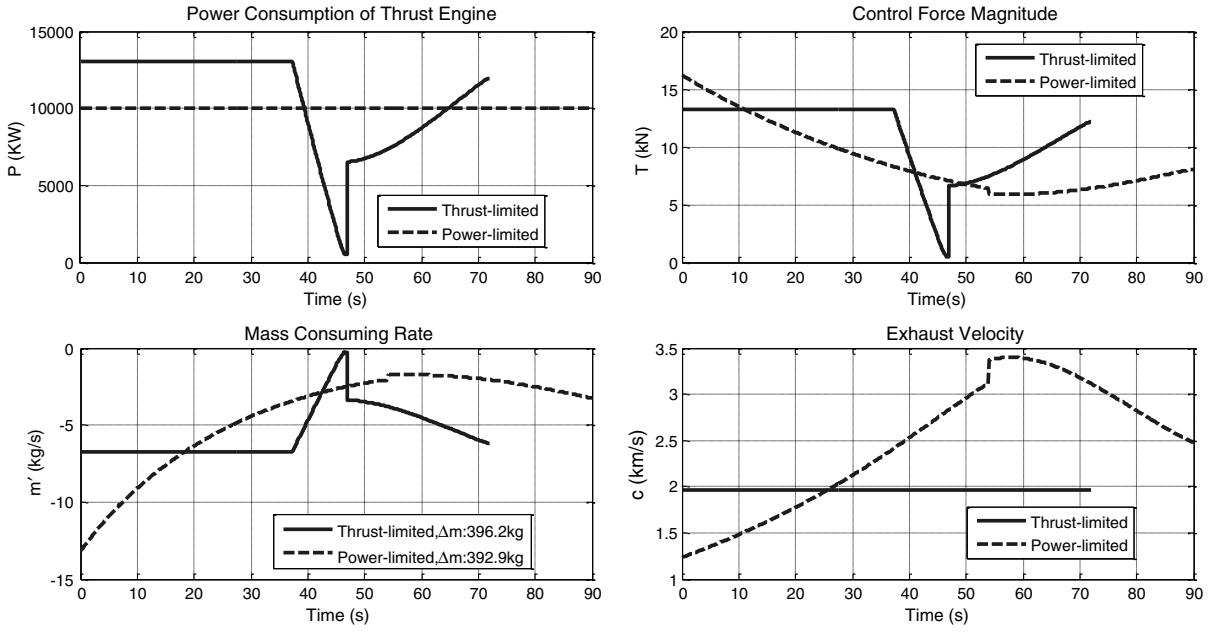

Fig. 2 Engine performance histories for waypoint-optimized Mars landing.

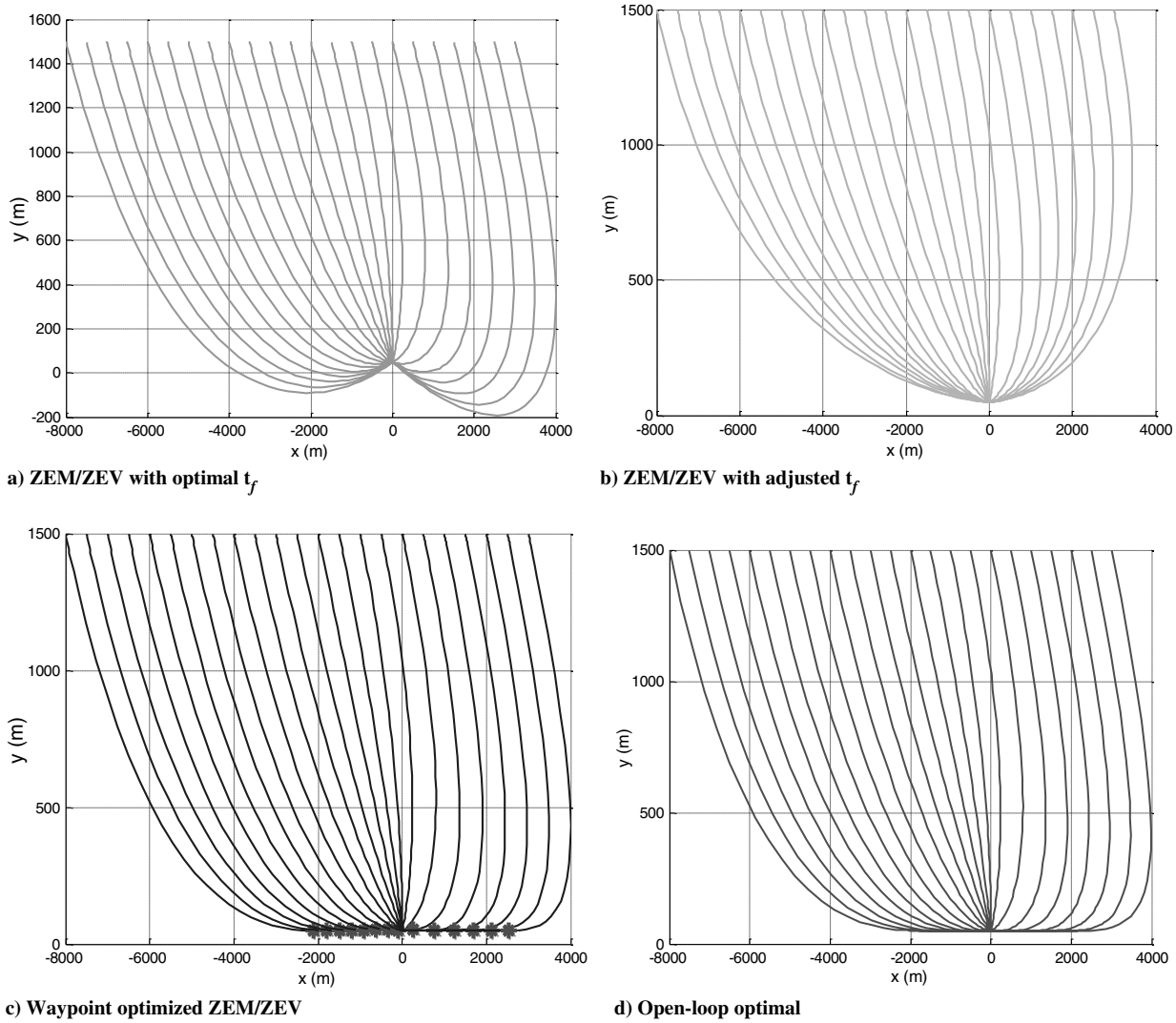

Fig. 3 Vehicle trajectories using various methods (power-limited engine).

lander can descend straight down onto the landing site. Figure 3 shows the optimal trajectories for a variety of initial conditions. Three different ZEM/ZEV methods are shown, as well as the open-loop optimal solution. The four control schemes are:

1) *ZEM/ZEV with Optimal* t_f (Fig. 3a): The standard ZEM/ZEV algorithm is employed, using the calculated optimal time, with no constraints. For many of the initial positions considered, the optimal trajectory passes through the surface, even with the 50 m "cushion."

2) *ZEM/ZEV with Adjusted* t_f (Fig. 3b): The standard ZEM/ZEV algorithm is again used, but the upper bound on flight time is enforced for cases that would violate the no-subsurface flight constraint. All of the trajectories for this case stay above the surface.

3) *Waypoint-Optimized ZEM/ZEV* (Fig. 3c): The quadratic programming problem is solved to determine the optimal waypoint, with t_f and t_m determined following the suggested procedure. The waypoints for each trajectory are shown as asterisks. All trajectories again stay above the surface. Other altitude constraints can be added by modifying the inequality constraints.

4) *Open-Loop Optimal* (Fig. 3d): The optimal solution, found by GPOPS, and satisfying the altitude constraint. These optimal trajectories look nearly identical to the waypoint-optimized ZEM/ZEV trajectories.

For some initial conditions, the basic ZEM/ZEV algorithm works without violating the altitude constraint. For other cases, either the mission time needs to be adjusted or a waypoint must be added. The performance of the various control schemes must ultimately be evaluated by comparing either the performance index J or the fuel usage Δm. Figure 4 shows the performance of each of the four algorithms in terms of J. The trends in Δm are similar and are not shown here. The mission time t_f is also shown. For initial conditions with horizontal range approximately between -4.5 and 0.5 km, the lander starts out "headed in the right direction," and all four schemes show almost identical performance. Outside of this range, the effectiveness of the waypoint-optimized ZEM/ZEV algorithm is apparent. For these cases, the scheme with adjusted t_f uses significantly more fuel than the optimal solution. ZEM/ZEV with optimal t_f performs nearly as well as the optimal solution, but for these cases the no-subsurface flight condition is violated, resulting in mission failure. The waypoint-optimized ZEM/ZEV algorithm achieves near-optimal performance while satisfying the constraint. In other words, for a variety of initial conditions, the proposed waypoint scheme achieves almost identical performance with the open-loop optimal solution.

B. Mars Landing with Thrust-Limited Engine

Unlike for a power-limited engine, for a thrust-limited engine, minimizing J is not equivalent to minimizing Δm. Furthermore, due to the nonlinear constraint on control acceleration, the optimal flight time found from step 2 does not guarantee an optimal J. Although the proposed ZEM/ZEV approach is not intended to be fuel-optimal, we will consider fuel usage to be the performance measure of interest, because it is of interest in any practical mission.

For the simulations shown, the spacecraft model is similar to that discussed in [4]. The maximum control force from the thrusters is assumed to be 16.753 kN, of which only 80% is available for control

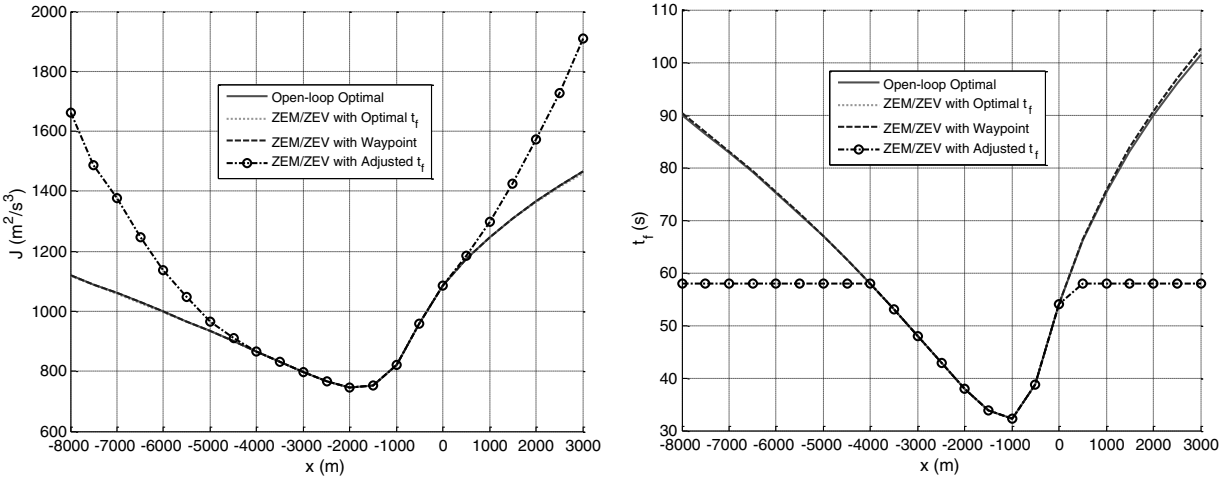

a) Performance index J (m^2/s^3) **b) Total flight time t_f (s)**

Fig. 4 Performance comparison of ZEM/ZEV and open-loop methods (power-limited engine).

(leaving a conservative margin). The engine exhaust velocity c is fixed at 1.964 km/s ($1/c = 5.09 \times 10^{-4}$ s/m.

Equation (19), used to determine the upper bound of t_f, does not take into account saturation constraints. The method of adjusting t_f does not work well in general. Typically, t_f is decreased to force a "straight shot" and avoid violating the no-subsurface flight constraint. However, fulfilling the same mission in less time usually requires higher acceleration levels during the mission. Adjusting the flight time downward to avoid collision thus results in control saturation.

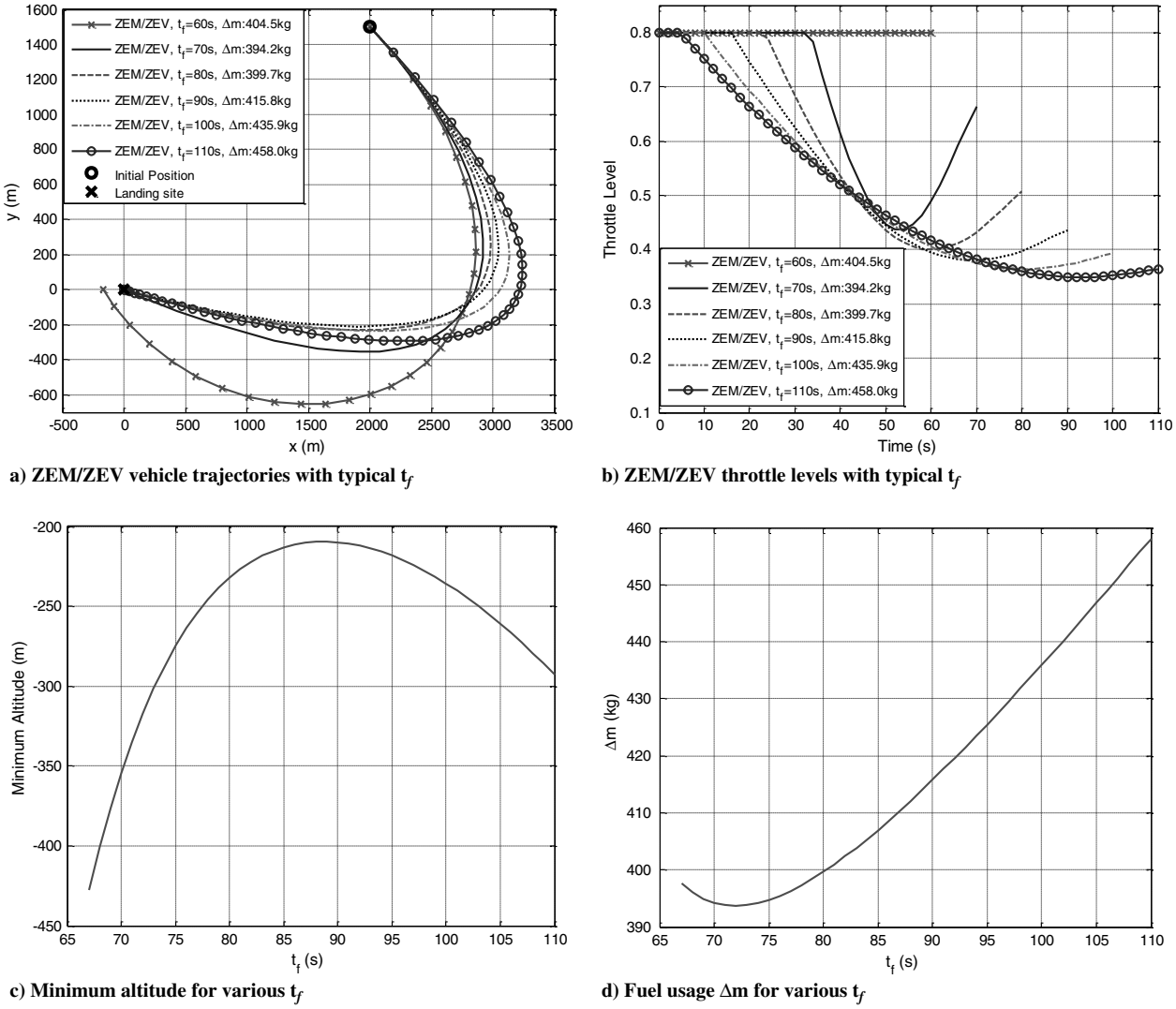

a) ZEM/ZEV vehicle trajectories with typical t_f **b) ZEM/ZEV throttle levels with typical t_f**

c) Minimum altitude for various t_f **d) Fuel usage Δm for various t_f**

Fig. 5 Performance of ZEM/ZEV algorithm with various flights times (thrust-limited engine).

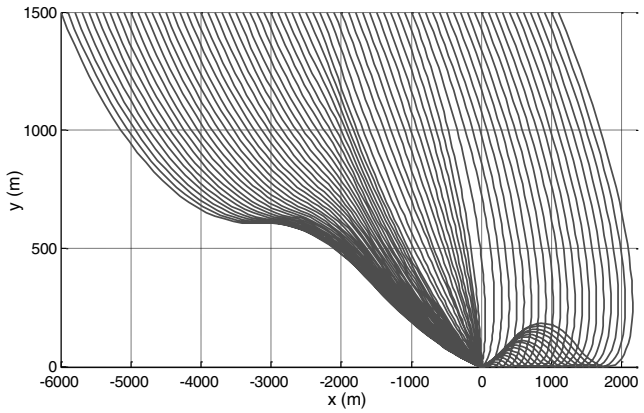

Fig. 6 Fuel-optimal vehicle trajectories (thrust-limited engine).

Figure 5 shows vehicle trajectories and throttle level histories for various mission times for the ZEM/ZEV algorithm and corresponding minimum altitudes and fuel usage. When the flight time is less than 67 s, the controls are saturated the entire time, and the terminal requirements are not met. By increasing the flight time above 67 s, the vehicle can successfully meet the terminal requirements, but the no-subsurface constraint is violated. For all times tested, the minimum altitude is below the surface. Fuel usage increases with increasing flight time, but even setting aside concerns on fuel usage, the landing mission cannot be accomplished solely by adjusting t_f.

Figure 6 shows a family of fuel-optimal solutions for a vehicle with a thrust-limited engine. For these initial conditions, the initial velocity and altitude are held constant, and the initial horizontal range is varied. These results can be obtained either by directly using TOMLAB optimization software, or by solving a second-order cone problem using the SeDuMi software package [4]. GPOPS can also be used to find these results, but for this particular problem GPOPS requires more computational time. From the family of trajectories shown, it is seen that when the landing site is ahead of the vehicle, the fuel-optimal trajectories converge inside an envelope before landing. When the landing site is behind the vehicle's initial position, the optimal trajectory turns around, then touches the surface, before turning upward and finally landing. These trajectories also converge on an envelope on the final approach.

The waypoint optimization scheme was examined for the case where simply adjusting t_f fails. From Fig. 5, it can be seen that the optimal t_f is 72 s. The corresponding time of minimum altitude is 47 s, chosen for t_m. Figure 7 shows the vehicle trajectories and throttle histories for the standard ZEM/ZEV algorithm, the ZEM/ZEV waypoint method, and the open-loop optimal solution. By using GPOPS to find an optimized waypoint, the ZEM/ZEV waypoint method successfully completes the landing mission in the presence of control saturation and a no-subsurface flight constraint. The fuel-optimal throttle shows the classical bang-off-bang form, resulting in fuel usage of 387.7 kg. The ZEM/ZEV waypoint algorithm uses 396.2 kg, only 2.2% more. Figure 2, previously shown, also provides detailed engine performance histories for the case with one waypoint, shown as a dotted line in Fig. 7. The piecewise nature of the control, with a jump at the waypoint, is easily seen.

To demonstrate the effectiveness of the proposed ZEM/ZEV waypoint strategy for a range of initial conditions, the initial position was varied, as in the last section. The initial velocity and altitude are held constant, while the initial horizontal position ranges from -8 to 3 km. A 50 m minimum altitude is imposed to avoid collision with surface hazards, making the final position $\mathbf{r}_f = (0, \quad 50, \quad 0)$ m. From here the lander can descend straight down onto the landing site. Figure 8 shows the optimal trajectories for a variety of initial conditions. Two ZEM/ZEV methods are shown, as well as the open-loop optimal solution. The three control schemes are:

1) *ZEM/ZEV with Optimal t_f to Minimize Δm* (Fig. 8a): The dynamic system is numerically propagated using the ZEM/ZEV algorithm. A Newton iteration method is used to find the t_f that minimizes Δm. For initial horizontal ranges from -8 to -1 km successfully complete the mission, while initial ranges larger than -1 km violate the no-subsurface flight constraint.

2) *Waypoint-Optimized ZEM/ZEV* (Fig. 8b): Fuel-optimal waypoints are found using GPOPS. Analytical derivatives are provided to GPOPS, using the differentiable saturation function in Eq. (38). The waypoints are shown as asterisks. The mission can be successfully carried out for all of the initial conditions shown.

3) *Open-Loop Fuel-Optimal* (Fig. 8c): The fuel-optimal results, similar to those shown in Fig. 3d, are generated by using either TOMLAB or SeDuMi.

The waypoint-optimized scheme results in trajectories that are qualitatively similar overall to the open-loop optimal trajectories, showing that adding one waypoint can change an infeasible ZEM/ZEV mission to a nearly optimal one. Figure 9 shows the fuel used and the total flight time for the various initial positions. The fuel usage from the waypoint method tracks very closely to the optimal, with slight variations at either extreme. The total mission times are also very close, showing that the waypoint method does approximate the open-loop optimal solution.

Based on the numerical tests shown here, the optimal waypoint can usually be found within $5 \sim 15$ s when t_f and t_m are fixed. When those times are free, the optimization takes longer and depends on the initial guess and range for each. Finding the optimal solution for a broad range of times can take up to a couple of minutes. For this reason, it is recommended that a fixed t_f and t_m are used.

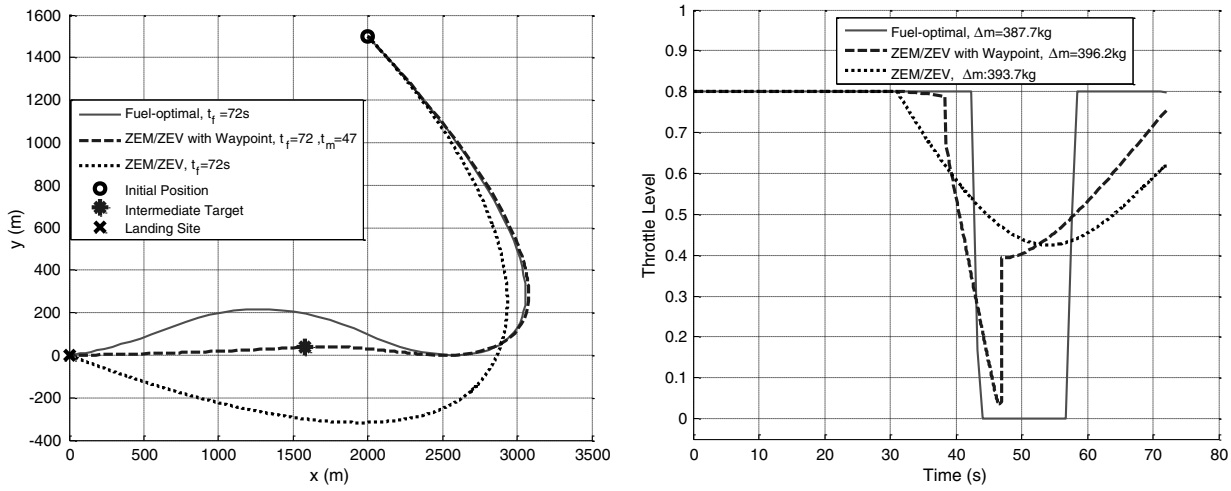

a) Vehicle trajectory **b) Throttle level**

Fig. 7 Comparison of ZEM/ZEV algorithm and fuel-optimal solution (thrust-limited engine).

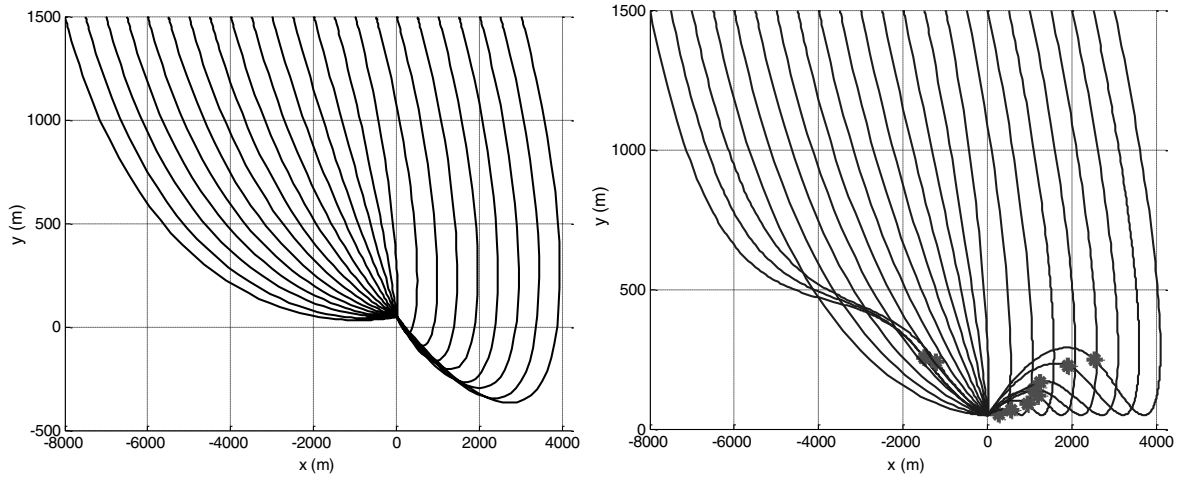

a) ZEM/ZEV with optimal t_f to minimize Δm

b) Waponit-optimized ZEM/ZEV

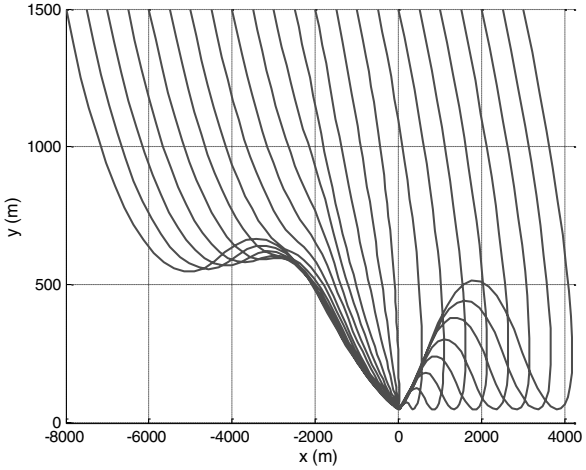

c) Open-loop fuel-optimal

Fig. 8 ZEM/ZEV and open-loop trajectories for minimizing Δm (thrust-limited engine).

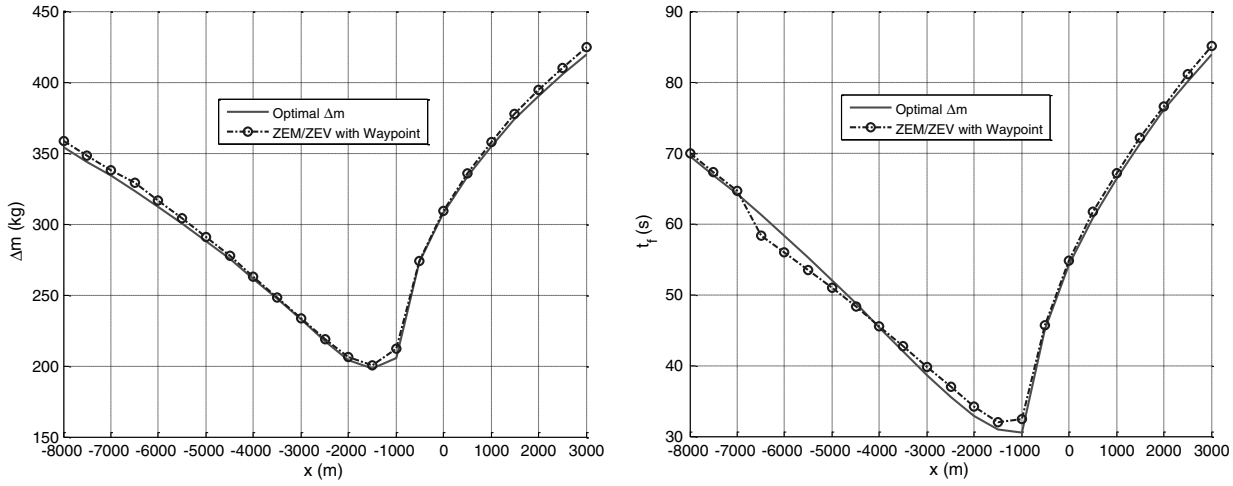

a) Performace index Δm

b) Total flight time

Fig. 9 Fuel-optimal solution and waypoint-optimized ZEM/ZEV (thrust-limited engine).

VII. Conclusions

This paper investigated the implementation of a zero-effort-miss/zero-effort-velocity (ZEM/ZEV) feedback guidance scheme for the powered descent phase of a Mars pinpoint landing mission. Two types of engines, power-limited and thrust-limited, were considered.

When a collision with the surface of Mars was predicted for the standard ZEM/ZEV algorithm, an intermediate waypoint was chosen using a numerical optimization program. The lander uses ZEM/ZEV feedback guidance to reach the waypoint, then uses ZEM/ZEV guidance to reach the landing site. For the power-limited engine, the control acceleration is not directly constrained, and so only a

minimum altitude constraint is considered. The waypoint optimization problem can be formulated as a standard quadratic programming problem. Several numerical optimization software packages can be used to solve this problem.

For the thrust-limited engine, a nonlinear saturation constraint is considered in addition to the no-subsurface flight constraint. The General Pseudospectral Optimal Control Software (GPOPS) package was used to find the optimal waypoint. A continuously differentiable approximation to the standard saturation function is introduced to provide analytical partial derivatives of various constraints with respect to states and controls, and these derivatives are passed to GPOPS to speed up the optimization process.

Numerical simulations for a few illustrative examples were performed. The ZEM/ZEV algorithms described in this paper were used, and the corresponding open-loop optimal solutions were found for comparison. Results show that constraints cannot be consistently satisfied solely by changing flight time. Instead, an optimized waypoint is used as an intermediate target for the ZEM/ZEV scheme. Comparison with the open-loop optimal solution shows that the waypoint method achieves near-optimal performance, while maintaining the desirable robustness properties of a feedback controller.

The waypoint-optimized ZEM/ZEV feedback guidance algorithm is more suitable for autonomous implementation than any purely open-loop method. The scheme requires only one waypoint to be stored, and the feedback nature is robust to disturbances. A real autonomous mission requires real-time computation of the optimal waypoint, starting from a range of possible initial conditions. A specialized optimizer for this problem is needed to ensure that the waypoint can be found quickly. Developing such an optimizer is a future research task.

Finally, the waypoint-optimized ZEM/ZEV algorithm is not restricted to Mars landing. In its most general form, it can be potentially apply to many other orbital maneuvering problems. A further detailed study of the application of the generalized ZEM/ZEV algorithm, both with and without a waypoint, can be found in [24].

Acknowledgments

This work was supported by a research grant from the Iowa Space Grant Consortium awarded to the Asteroid Deflection Research Center at Iowa State University. The authors would like to thank Ramanathan Sugumaran (Director of the Iowa Space Grant Consortium) for his support of this research project.

References

[1] Braun, R. D., and Manning, R. M., "Mars Exploration Entry, Descent and Landing Challenges," *Journal of Spacecraft and Rockets*, Vol. 44, No. 2, 2007, pp. 310–323. doi:10.2514/1.25116

[2] Wolf, A. A., Graves, C., Powell, R. W., and Johnson, W., "Systems for Pinpoint Landing at Mars," *14th AIAA/AAS Space Flight Mechanics Meeting*, AAS Paper 04-272, 2004.

[3] Desai, P. N., Prince, J. L., Queen, E. M., Cruz, J. R., and Grover, M. R., "Entry, Descent, and Landing Performance of the Mars Phoenix Lander," AIAA Paper 2008-7346, 2008.

[4] Açikmeşe, B., and Ploen, S. R., "Convex Programming Approach to Powered Descent Guidance for Mars Landing," *Journal of Guidance, Control, and Dynamics*, Vol. 30, No. 5, 2007, pp. 1353–1366. doi:10.2514/1.27553

[5] Blackmore, L., Açikmeşe, B., and Scharf, D. P., "Minimum-Landing-Error Powered-Descent Guidance for Mars Landing Using Convex Optimization," *Journal of Guidance, Control, and Dynamics*, Vol. 33, No. 4, 2010, pp. 1161–1171. doi:10.2514/1.47202

[6] Ebrahimi, B., Bahrami, M., and Roshanian, J., "Optimal Sliding-Mode Guidance with Terminal Velocity Constraint for Fixed-Interval Propulsive Maneuvers," *Acta Astronautica*, Vol. 62, Nos. 10–11, 2008, pp. 556–562. doi:10.1016/j.actaastro.2008.02.002

[7] Furfaro, R., Selnick, S., Cupples, M. L., and Cribb, M. W., "Non-Linear Sliding Guidance Algorithms for Precision Lunar Landing," *21st AAS/AIAA Space Flight Mechanics Meeting*, AAS Paper 11-167, 2011.

[8] Hawkins, M., Guo, Y., and Wie, B., "Guidance Algorithms for Asteroid Intercept Missions with Precision Targeting Requirements," *AAS/AIAA Astrodynamics Specialist Conference*, AAS Paper 11-531, 2011.

[9] Guo, Y., Hawkins, M., and Wie, B., "Optimal Feedback Guidance Algorithms for Planetary Landing and Asteroid Intercept," *AAS/AIAA Astrodynamics Specialist Conference*, AAS Paper 11-588, 2011.

[10] Bryson, A. E., and Ho, Y.-C., *Applied Optimal Control*, Wiley, New York, 1969, pp. 154–155.

[11] Battin, R. H., *An Introduction to the Mathematics and Methods of Astrodynamics*, AIAA Education Series, AIAA, New York, 1987, pp. 558–561.

[12] D'Souza, C. N., "An Optimal Guidance Law for Planetary Landing," AIAA Paper 1997-3709, 1997.

[13] Steinfeldt, B. A., Grant, M. J., Matz, D. A., Braun, R. D., and Barton, G. H., "Guidance, Navigation, and Control System Performance Trades for Mars Pinpoint Landing," *Journal of Spacecraft and Rockets*, Vol. 47, No. 1, 2010, pp. 188–198. doi:10.2514/1.45779

[14] Sharma, R., Vadali, S. R., and Hurtado, J. E., "Optimal Nonlinear Feedback Control Design Using a Waypoint Method," *Journal of Guidance, Control, and Dynamics*, Vol. 34, No. 3, 2011, pp. 698–705. doi:10.2514/1.52470

[15] Elnagar, G., Kazemi, M., and Razzaghi, M., "The Pseudospectral Legendre Method for Discretizing Optimal-Control Problems," *IEEE Transactions on Automatic Control*, Vol. 40, No. 10, 1995, pp. 1793–1796. doi:10.1109/9.467672

[16] Huntington, G. T., and Rao, A. V., "Optimal Reconfiguration of Spacecraft Formations Using the Gauss Pseudospectral Method," *Journal of Guidance, Control, and Dynamics*, Vol. 31, No. 3, 2011, pp. 689–698. doi:10.2514/1.31083

[17] Rao, A. V., Benson, D. A., Darby, C., Patterson, M. A., Francolin, C., Sanders, I., and Huntington, G. T., "Algorithm 902: GPOPS, A MATLAB Software for Solving Multiple-Phase Optimal Control Problems Using the Gauss Pseudospectral Method," *ACM Transactions on Mathematical Software*, Vol. 37, No. 2, 22 April 2010, pp. 1–39. doi:10.1145/1731022.1731032

[18] Karpenko, M., Bedrossian, N., Bhatt, S., Fleming, A., and Ross, I. M., "First Flight Results on Time-Optimal Spacecraft Slews," *21st AAS/AIAA Space Flight Mechanics Meeting*, AAS Paper 11-110, 2011.

[19] Holmstrom, K., Goran, A. O., and Edvall, M. M., "User's Guide for TOMLAB 7," http://tomopt.com/docs/TOMLAB.pdf [accessed Oct. 2011].

[20] Rao, A. V., Benson, D. A., Darby, C., Mahon, B., Francolin, C., and Patterson, M. A., "User's Manual for GPOPS Version 4.x: A MATLAB Software for Solving Multiple-Phase Optimal Control Problems Using hp-Adaptive Pseudospectral Methods," http://www.gpops.org/gpopsManual.pdf [accessed Oct. 2011].

[21] Seifert, H. ed., *Space Technology*, Wiley, New York, 1959, Chaps. 9–10.

[22] Prussing, J. E., "Equation for Optimal Power-Limited Spacecraft Trajectories," *Journal of Guidance, Control, and Dynamics*, Vol. 16, No. 2, 1993, pp. 391–393. doi:10.2514/3.21017

[23] Conway, B. ed., *Spacecraft Trajectory Optimization*, Cambridge Univ. Press, Cambridge, England, U.K., 2010, pp. 61–62, Chaps. 2–3.

[24] Guo, Y., Hawkins, M., and Wie, B., "Applications of Generalized Zero-Effort-Miss/Zero-Effort-Velocity Feedback Guidance Algorithm," *22nd AAS/AIAA Space Flight Mechanics Meeting*, AAS Paper 12-197, 2012.